Radial velocity mapping of Paczyński's star AW UMa: not a contact binary[⋆]

T. Pribulla[1,2]† and S. M. Rucinski[2]†

[1]*Astronomical Institute of the Slovak Academy of Sciences, 05960 Tatranská Lomnica, The Slovak Republic*
[2]*Department of Astronomy and Astrophysics, University of Toronto, 50 St George Street, Toronto, Ontario, Canada M5S 3H4*

ABSTRACT

We present 2D (radial velocity, orbital phase) spectroscopic results for the very low mass-ratio close binary AW UMa which strongly indicate that the spectroscopic mass ratio ($q_{sp} = 0.10$) does not agree with the photometrically derived one and that the widely adopted contact binary model appears to experience serious inconsistencies and limitations for this object. AW UMa is compared with V566 Oph ($q_{sp} = 0.26$) which we found to behave according to the contact model. Observed broadening functions of AW UMa can be interpreted by a very strong limb darkening and/or non-solid-body rotation of the dominant primary component; the former assumption is unphysical while the differential rotation is not supported by an apparent stability of localized, dark features on the outer side of the primary. There are indications of the existence of an equatorial belt encompassing the whole system. All deficiencies in the interpretation and the discrepancy between the photometric and spectroscopic mass ratio of AW UMa can be solved within a new model of AW UMa where both components are detached and the system is submerged in a stream of hot, optically thick matter which mimics the stellar contact. While the masses and their ratio are correctly given by spectroscopy, the photometric picture is heavily modified by the matter engulfing both stars in the equatorial plane.

Key words: binaries: eclipsing – binaries: spectroscopic.

1 INTRODUCTION

Most of the light-curve analyses of contact binary stars of the W UMa type assume – following the seminal papers of Lucy (1968a,b) – that shapes of these stars are well described by a common equipotential surface of the Roche model. However, light-curve analyses have a common limitation: a light curve is a result of a mapping of a complex 3D surface into a 1D function of time. The information content of many contact binary light curves is low, particularly when total eclipses do not occur. The correctness of the assumed model is of a crucial importance for a proper interpretation of these binaries and still remains an open issue.

The exact solid-body rotation of the Roche model is a strong assumption of the Lucy model. While it is a convenient simplification of the problem, we have no theoretical basis to believe that a strictly solid-body rotation is really present. The Sun does not rotate rigidly and there are many indications that other solar type stars also rotate differentially. We have rather vague ideas for rotation rates some hundred times than the solar. Simple arguments based on the presence of horizontal temperature gradients could be used to argue that convection cells should break into small ones leading to an enhanced turbulent viscosity and thus a solid-body rotation. But – on the other hand – the large difference in the component nuclear energy production requires an effective transport over common envelope which cannot happen without extensive horizontal motions. Also, the degree of the solid-body rotation may depend on the mass of the secondary component; when it is very small, its tidal influence may be too weak to prevent the big primary from rotating differentially.

Within the Roche model, a common equipotential surface has a relatively simple shape and is described by only three free geometrical parameters (the mass ratio, q, the degree of contact, F and the inclination, i); this parametric description is even simpler than for detached binaries where sizes of components are unrelated. All extant solutions of contact binary light curves still require a proof of the strict applicability of the Roche model described in such simple terms.

In this paper we attempt to lift the degeneracy of the 3D into 1D light-curve mapping by using the broadening function (BF) formalism (Rucinski 2002). A BF gives the surface brightness distribution of a stellar object in the velocity space. This is true if all surface points radiate the same spectrum, which appears to be a particularly valid assumption for contact binaries (see Anderson, Standford &

Leininger 1983). In the case of a solid-body rotation, the observed radial velocity is proportional to the projected distance from the axis of rotation. When combined with the uniform surface brightness, a single BF gives a 1D image of system in the velocity space. We go one step further and analyse several BFs by arranging and combining them in the orbital phase into 2D functions (radial velocity, orbital phase), effectively the phase dependent, 2D radial velocity maps of a binary system. The approach of arranging spectra in the phase domain, when the phase coherence is an issue, has already been used by several researches, particularly to study rapid changes in cataclysmic variables. In the David Dunlap Observatory (DDO) studies of the binary stars, it was used mostly as an auxiliary tool (Rucinski et al. 2005; Pribulla et al. 2006, 2007) for faint binaries where individual BFs were poor and some phase averaging was advantageous. But here, it is used as the main way to assess correctness of the solid-body rotation and to analyse the well observed contact binary AW UMa.

The main object of our study, AW UMa, is presented in Section 2. The observations are described in Section 3 while the determination of radial velocities through a Gaussian and rotational profile fitting and through direct modelling of the BFs is presented in Section 4. The resulting spectroscopic elements and the absolute parameters are presented in Section 5. Sections 6 and 7 discuss the critical issue of the applicability of the Roche model and of the deviations from it that we have discovered. A new model of AW UMa is presented and discussed in Section 8. The results are summarized in Section 9. Throughout the paper V566 Oph is discussed as a comparison object for AW UMa; this contact binary was previously analysed in Pribulla et al. (2006).

2 AW UMA

After the discovery of AW UMa by Paczyński (1964) and after the important demonstration by Mochnacki & Doughty (1972a) that its photometric variability beautifully agrees with the then recently developed contact model of Lucy (1968a,b) – this being true in spite of its unexpectedly small value of the photometrically derived mass ratio $q \simeq 0.07$–0.08 – the binary has played a special role in the field of contact binaries. Its very small photometric mass ratio was reconfirmed several times (for references to observational studies, see Pribulla et al. 1999). Throughout the development of the field, all theoretical studies had to include this object as a crucial if extreme datum in all structural and evolutionary modelling efforts. The key point was that even at this extreme mass ratio, with the almost totally energetically inert secondary component, the surface temperature can be equalized over the whole common envelope as described by an equipotential surface of the Roche model.

The particularly good characterization of the light curve and the seemingly unambiguous conclusion that $q \simeq 0.07$–0.08 were a direct result of the presence of total eclipses strongly constraining the parameter space of the contact model solutions. While the photometric observations leave very little room for questioning the low value of q for AW UMa – as long as it really fulfils all conditions of the Lucy model – spectroscopic data were less easy to interpret. This is because the spectral lines of the primary component are broad and show a very small and difficult to measure orbital variability with the semi-amplitude of the variation, K_1, which is *several times smaller* than the rotational broadening of its lines. The spectral signature of the secondary component, while nowadays rather easily detectable, is weak indicating $L_2/L_1 \sim 0.1$ in the visual region. As the result, the spectroscopic elements of AW UMa remain virtually undetermined in spite of several previous attempts.

Paczyński (1964) was not able to detect the secondary component and determined orbital parameters of the primary component only by measuring positions of H_γ and H_δ on photographic spectra with a (low) dispersion of 75 Å mm^{-1}; this resulted in $V_0 = -1 \pm 2$ km s^{-1} and $K_1 = 28 \pm 3$ km s^{-1}. McLean (1981) used spectra of a higher dispersion (20 Å mm^{-1}) and applied the cross-correlation technique. He marginally detected the secondary component and gave very preliminary spectroscopic elements: $V_0 = -17 \pm 7$ km s^{-1}, $K_1 = 29 \pm 8$ km s^{-1} and $K_2 = 423 \pm 80$ km s^{-1}.

Rensing, Mochnacki & Bolton (1985) were able to measure the radial velocities of the primary component stacking Doppler profiles of selected lines. Their low value of $K_1 = 22.2 \pm 0.9$ km s^{-1} alleviated the previous problem of the unexpectedly large total mass ($M_1 + M_2 \sim 4 \, M_\odot$) which had resulted from a relatively large semi-amplitude K_1 and the (assumed) small mass ratio. Unfortunately, the exposure times of the spectra were very long (4.7–11.2 per cent in phase) which resulted in smearing of the spectral lines and a reduction of K_1. An important point stressed by Rensing et al. (1985) was that the spectral lines were too narrow when compared with the Lucy model predictions. Even the hydrogen lines were narrow, which was difficult to interpret in any reasonable way; the authors considered problems with the continuum placement as a cause which could indeed be magnified when working with photographic spectra. This 'narrow line problem' had been noticed by several researchers (Mochnacki & Doughty 1972a; Anderson et al. 1983) but – because it did not affect the photocentre velocities – it remained an unexplained curiosity.

The first high-quality CCD spectra and their analysis were presented by Rucinski (1992a) who developed the new BF technique for this star. Even with the good-quality spectroscopic data, it was impossible to reliably determine the full set of parameters. For that reason Rucinski (1992a) chose to fix q at the photometric value, determining only the overall velocity span, $K_1 + K_2$. The data appeared to confirm the contact model, but some latitude in the selection of the best mass ratio q by 0.005 around 0.075 resulted in an uncomfortably large range in total mass, $M_1 + M_2$. Finally, Pribulla et al. (1999) obtained new photographic spectra and reanalysed all published radial velocities. Subtraction of line profiles between the two quadratures indicated $q \approx 0.08$. The authors tried to explain the differences in previously determined systemic velocity V_0 by the multiple nature of AW UMa and the centre-of-mass motion.

The current study has been mostly driven by our realization that new high-quality spectroscopic data obtained at the DDO for AW UMa do not confirm the low value of the mass ratio suggesting a larger value, closer to $q \simeq 0.10$. The seemingly small change in the mass ratio from $\simeq 0.08$ to $\simeq 0.10$ is important. Not only that it strongly affects the final value of the total mass of the system, $M_1 + M_2$, by controlling M_1, but also – as recently shown by Paczyński, Sienkiewicz & Szczygieł (2007) – it is practically impossible to obtain a stable structural model for AW UMa for $q < 0.1$ and – even then – the secondary turns out to be a very unusual object with a very small core and a tenuous, low-density envelope.

With the mass ratio being such an important parameter, we decided to compare the BFs of AW UMa with identically obtained data for the contact system V566 Oph. This binary is very similar in spectral type, orbital period and brightness to AW UMa, but its mass ratio is larger, $q_{ph} \simeq 0.24$ (Mochnacki & Doughty 1972b), $q_{sp} = 0.26 \pm 0.01$ (Pribulla et al. 2006). It is also a totally eclipsing system, a condition which very strongly constrains and improves parametric solutions. The V566 Oph data utilized in the current paper were already presented in Pribulla et al. (2006) and are discussed here only when directly relevant for the discussion of AW

Table 1. Properties of AW UMa and V566 Oph.

HD	99946	163611
HIP	56106	87860
π (mas)	15.13(0.90)	13.98(1.11)
V_{max}	6.83	7.46
V_{min}	7.13	7.96
$B - V$	0.33	0.41
M_V	2.74(12)	3.20(16)
M_V (RD)	2.70	3.08
Spectral type	F0V–F1V	F4V
Period (d)	0.438 7258	0.409 6546
T_0(HJD)	2 450 124.9954	2 451 314.0094

The values of the period and of $T_0 - 240\,0000$ were used for calculating phases of the spectroscopic observations. Absolute visual magnitude, M_V, was determined using the *Hipparcos* parallax, while M_V (RD) is absolute magnitude estimated using calibration of Rucinski & Duerbeck (1997) from observed colour and period. Standard errors of some parameters are given in parentheses.

Table 2. Journal of spectroscopic observations of AW UMa and V566 Oph.

Object	Spectrum	HJD 2 400 000+	Phase	Exp.	ADU
AW UMa	K0022717	53785.9046	0.9222	902	48941
AW UMa	K0022718	53785.9165	0.9494	901	40397
AW UMa	K0022720	53785.9291	0.9782	902	44140
AW UMa	K0022721	53785.9398	0.0026	901	40923
AW UMa	K0022723	53785.9516	0.0295	902	39354
AW UMa	K0022730	53785.9788	0.0914	825	33179
AW UMa	K0022882	53789.8271	0.8630	374	27166
AW UMa	K0022883	53789.8325	0.8752	487	23001
AW UMa	K0022884	53789.8408	0.8940	901	15881
AW UMa	K0022938	53790.5965	0.6167	546	28549

Explanation of columns: Spectrum – original FITS file name; HJD – Heliocentric Julian Date of mid-exposure; Phase – phase of mid-exposure; Exp. – exposure time in seconds; ADU – median level of the extracted spectrum in ADU. The full table is available in the electronic form only. Phases correspond to optimal ephemerides in Table 4 (for AW UMa according to the solution with $u_1 = 1.00$ and $u_2 = 0.56$).

UMa. We summarize the essential properties of both systems in Table 1.

Neither AW UMa nor V566 Oph has close companions. We checked AW UMa carefully and see no very close body which would show in radial velocity centre-of-mass velocities. We see also no spectral signatures of a K- or M-type dwarf star in our spectra while unpublished CFHT adaptive optics observations (see Pribulla & Rucinski 2006) did not reveal any close visual companions at separations >0.2 arcsec. AW UMa forms a common proper-motion pair with BD+30°2164 at an angular separation of about 67 arcsec. The radial velocity of the companion, -13.28 ± 0.39 km s^{-1} (Tokovinin & Smekhov 2002), is very close to the centre of mass velocity of AW UMa. The proper-motion velocity components for both stars are also similar: According to the *Hipparcos* Tycho project (Høg et al. 2000), $\mu_\alpha \cos \delta = -82.8(9)$ and $-82.0(16)$ mas yr^{-1} and $\mu_\delta = -199.3(9)$ and $-198.6(15)$ mas yr^{-1}, for AW UMa and BD+30°2164, respectively. While the presence of the distant companion of AW UMa has no direct relevance to our discussion, it does help in constraining the absolute magnitude of AW UMa at $M_V \simeq 2.5$ (assuming $B - V = 0.72$ for the G5 main sequence companion of AW UMa) which indicates the spectral type of A9V/F0V. The spectral type of AW UMa is very hard to estimate directly because of the strong broadening of the spectral lines; it is most often quoted as F0/2V.

3 OBSERVATIONS

All discussed here observations of AW UMa were obtained using the slit spectrograph in the Cassegrain focus of 1.88-m telescope of the DDO. The spectra were taken in a window of about 240 Å around the Mg I triplet (5167, 5173 and 5184 Å) with an effective resolving power of about 12 000–14 000. The journal is given in Table 2. Two different diffraction gratings were used, with 1800 and 2160 lines mm^{-1}, with the same effective spectral resolution, but with a different sampling per pixel (0.145 and 0.117 Å pixel^{-1}). 1D spectra were extracted by the usual procedures within the IRAF environment[1] after the bias subtraction and the flat-field division.

Cosmic ray trails were removed using a program provided by Pych (2004). BFs were extracted by the method described in Rucinski (1992a) using, as templates, spectra of slowly rotating standard stars of similar spectral type (see below).

AW UMa was observed on 12 nights of 2006 February 18/19 to April 15/16 and on 2007 April 9/10 using the 2160 lines mm^{-1} grating. In total, 109 spectra uniformly covering the orbital cycle of the binary were obtained. The exposure times varied between 5.5 and 15 min (0.9–2.4 per cent of the orbital period). The star HD 128167 (σ Boo, F2V, $V \sin i = 5$ km s^{-1}, $V_r = +0.2 \pm 0.9$ km s^{-1}) served as the BF template. As expected, the use of a different template (HD 222368, ι Psc, F7V) resulted in very similar BFs.

V566 Oph was observed on six nights between 2005 May 5/6 and June 22/23 with the 1800 lines mm^{-1} grating. These data are described in Pribulla et al. (2006). Later, the system was observed using the 2160 lines mm^{-1} grating on four nights between 2005 August 22/23 and 2005 September 18/19; in total, 57 spectra were observed. HD 222368 (F7V, $V \sin i = 3$ km s^{-1}, $V_r = +5.4$ km s^{-1}) was used as a template.

For a direct comparison, the BFs for AW UMa and V566 Oph were extracted with the same step in radial velocity and were smoothed by convolving with the Gaussian function of $\sigma = 1.5$ bin in radial velocity corresponding to 10 km s^{-1}. A 2D (radial velocity, orbital phase) map of AW UMa was constructed by sorting the available 109 BFs in phase, rebinning them with a phase step of 0.01 and, finally, smoothing by a convolution with the Gaussian function of $\sigma = 0.01$ in phase; the corresponding map for V566 Oph, because of fewer observations, was constructed using the phase step of 0.02. The map for AW UMa, in Fig. 1, clearly shows the orbital motion of both components. The transit of the secondary component is seen as a dark streak cutting through the profile of the primary. Here we see the first but important deviation from the model in that the width of the secondary in the velocity space is much narrower during the transit than could be expected from its appearance at the orbital quadratures; it is also asymmetric as the two limb-darkened 'edges' of the secondary are not equally deep. There exists also a marked difference of the BFs between the two quadratures which we discuss in Section 7). We note that the phased BFs reveal presence of faint, localized, dark features on the primary component drifting at the star rotation rate which are best visible as diagonal streaks around
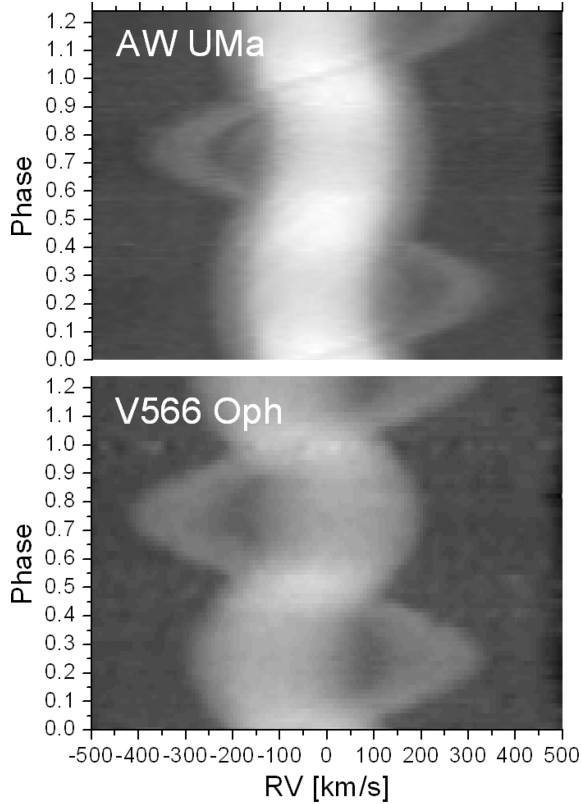
---

[1] IRAF is distributed by the National Optical Astronomy Observatories, which are operated by the Association of Universities for Research in Astronomy, Inc., under cooperative agreement with the NSF.

Figure 1. The grey-scale plot of the BFs of AW UMa (top) and V566 Oph (bottom). The BFs were rebinned to equal intervals in the phase and then Gaussian smoothed (see the text for details). Residuals from two considered models are shown in Figs 5 and 9.

phases 0.3–0.55. We will speculate that these are photospheric spots which remained stable over one year of the AW UMa observing.

4 RADIAL VELOCITIES AND MODELING OF THE BROADENING FUNCTIONS

Because of the extreme mass ratio, AW UMa is a difficult object for radial velocity determination from the BFs, in the way described by Rucinski (1992a). All problems encountered for contact binaries appear in this case in their most elevated form so that their brief summary may be in order.

There exist several ways to determine radial velocities from the BFs. The simplest and entirely model-independent one is through fitting of Gaussian profiles to the peaks in the BFs. This technique has been successfully used throughout the DDO series of spectroscopic element determination for 90 binaries, see the DDO papers Lu & Rucinski (1999) to Rucinski et al. (2005). Unfortunately the Gaussian profiles do not really represent the expected shapes of the BFs and are just a convenient numerical tool. Starting with the paper Pribulla et al. (2006), we have been using the rotational profiles. The theoretical rotational profiles slightly depend on the limb darkening (which can be fixed at a reasonable value) but – operationally – are very similar to Gaussians. Effectively, this approach corresponds to an approximation of the binary components by limb-darkened spheres. Because of the sharp, almost vertical edges of such profiles, they appear to give more stable and consistent centroid results than the Gaussians.

Both, the Gaussians and the rotational profiles give the central positions of the fitted BF peaks, but neither of the approaches in-

cludes proximity and eclipse effects. The projected photocentres of binary components are close to their mass centres, but small asymmetries (such as the reflection effect, which is however small in contact binaries or ellipsoidal distortion asymmetries) remain and are not accounted for. Having the individual velocities determined, the spectroscopic orbital elements are determined by either fitting simple sine curves to the photocentric velocities or by modelling the BFs with the Roche model assumption leading to predictions how proximity effects may shift the light centroids.

Instead of fitting the individual components, the whole set of the available BFs can be simultaneously fitted by model BFs calculated using the Roche model. This approach is vastly more physical, but its major disadvantage is the large number of the parameters and complex interdependencies between them.

In the present paper we use all the above techniques to evaluate their effects on the spectroscopic orbit of AW UMa. For the Gaussian and the rotational profile fitting, we used the BFs away from the eclipses, beyond phases ± 0.12 from the eclipse centres. For the direct modelling, we used all the available BFs, including those within the eclipses. We evaluate the used techniques below in succession.

4.1 Gaussian profile fitting

A sum of two Gaussian functions was fitted to each BFs by adjusting seven parameters: the baseline level, intensities of both components, their radial velocity positions and widths. By intensities of components we mean their individual strengths in the BFs; their added integrals are expected to equal unity for a perfect spectral type match between the object (AW UMa) and the template.

4.2 Rotational profile fitting

In an approach similar to the Gaussian fitting, we added two rotational profiles to form one double-peaked profile; the limb-darkening coefficient for both components was set at the same value, $u_1 = u_2 = u$. Again there are seven parameters to fit: the baseline, intensities of both components, their radial velocity positions and half-widths. Because the BF peaks for AW UMa had a 'pointed' or 'triangular' shapes, unlike what is expected from rotation alone, we considered different values of u between $u = 0.2$ to 1.0. Unexpectedly, a measure of the global quality of the fit, the weighted sum of squares of residuals for all simultaneously fitted BFs, reached a minimum for an extreme value of $u = 1$. This is entirely incompatible with the spectral type of F0/2V at the wavelength 5184 Å where an appropriate value of the limb-darkening coefficient should be around 0.52 (Van Hamme 1993).

It should be noted that the global fit in u related mostly to the properties of the primary profile because the contribution of the secondary was small and its peak was hard to fit. When left to an automatic adjustment, the half-width of the secondary peak varied over a large range. We were forced to fix it at 70 km s^{-1} which provided globally the best fits. In the end, two values of limb-darkening coefficient, $u = 0.52$ and 1.00, were considered, the latter being unphysical but able to reproduce the data much better than the former.

While AW UMa clearly shows the very strange shape of its primary component in radial velocities (in BFs), in the case of V566 Oph the shapes of extracted BFs are consistent with the rotational profiles computed for the expected theoretical limb darkening of $u = 0.56$. We show typical BFs at the orbital quadratures in Fig. 2. The fits shown in the figure are for the contact model BFs, as described in Section 4.4. Attention is drawn to the peaked shape of the AW UMa primary and the presence of unexplainable 'kinks' in the
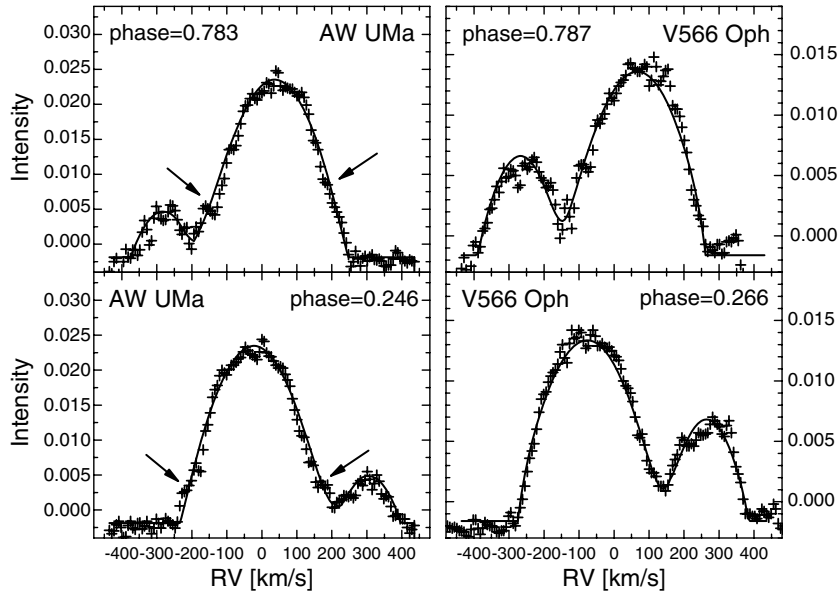
Figure 2. Fitting the model profiles to typical BFs of AW UMa and V566 Oph at the orbital quadratures. Note the relatively narrow and peaked shape of the AW UMa primary signature as well as the 'kinks' which broaden it below some 30 per cent above the baseline (indicated by arrows). The limb-darkening coefficient was fixed at the theoretically predicted values, 0.52 for AW UMa and 0.555 for V566 Oph. The slightly negative zero level of the BFs is due to difficulties with the true continuum placement of the heavily broadened spectra; the *shapes* of the BFs are unaffected, but they do suffer vertical shifts of an unknown size. This effect has also affected the BFs in Figs 7 and 9. We comment on this effect in item 4 of Section 7.

profile some 30 per cent above the baseline which are related to an additional broadening at the base.

We note in passing that we did not consider any of the non-linear forms of the limb darkening. This decision resulted mostly from the good reproduction of the V566 Oph BFs by predictions based on the linear limb darkening.

4.3 Rotational profiles modified for differential rotation

While an artificially large value of u can give a more peaked signature of the AW UMa primary, an entirely different explanation for such a shape can be sought in terms of the differential rotation of the solar type, with the polar regions moving slower than the equatorial regions. The simplest assumption of a dependence of the angular rotation velocity ω on the latitude b is

$$\omega(b) = \omega(0)(1 - \alpha \sin^2 b). \tag{1}$$

For simplicity and because of the geometry of AW UMa, we assumed that the equatorial $\omega(0)$ was always equal to the orbital rotation rate. With this assumption, $\alpha = 0$ corresponds to the solid-body rotation while $\alpha = 1$ corresponds to a strongly differential rotation with the non-rotating poles. The rotational profile with such a description for ω cannot be expressed as an analytical function and requires a numerical integration over the visible part of star even for a simplified case of the star retaining the spherical shape (such as the solar case). The effects of the limb darkening and the differential rotation for a spherical star are shown in Fig. 3. The shape of the rotational profile only weakly depends on the inclination of the rotation axis.

The rotational profiles with $\alpha > 0$ tend to reproduce the narrow shape of the primary in the BFs. A grid search for the best values of the limb-darkening coefficient u and the parameter α giving
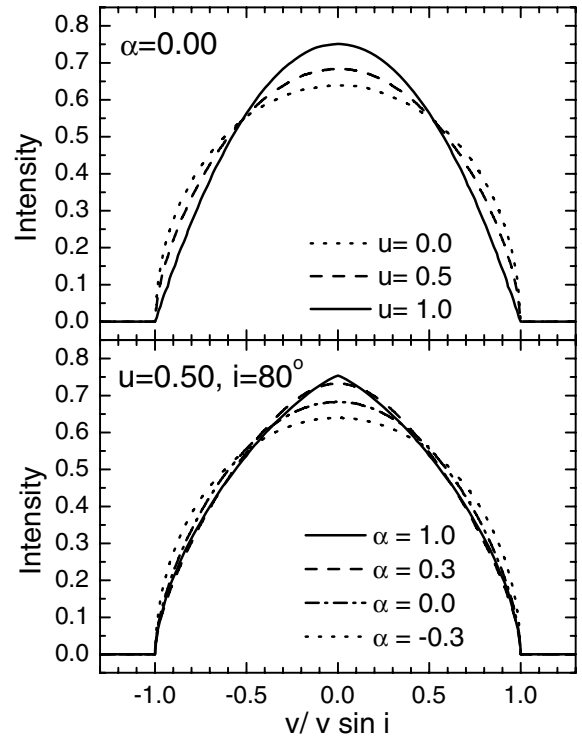

Figure 3. Effects of the varying limb darkening (top) and differential rotation (bottom) on the shape of the rotational profile of a single rotating star. The latitude (b) dependence of angular velocity was computed as $\omega(b) = \omega(0) [1 - \alpha \sin^2 b]$. In the case of a differential rotation, the shape of the rotational profile slightly depends on the inclination angle.
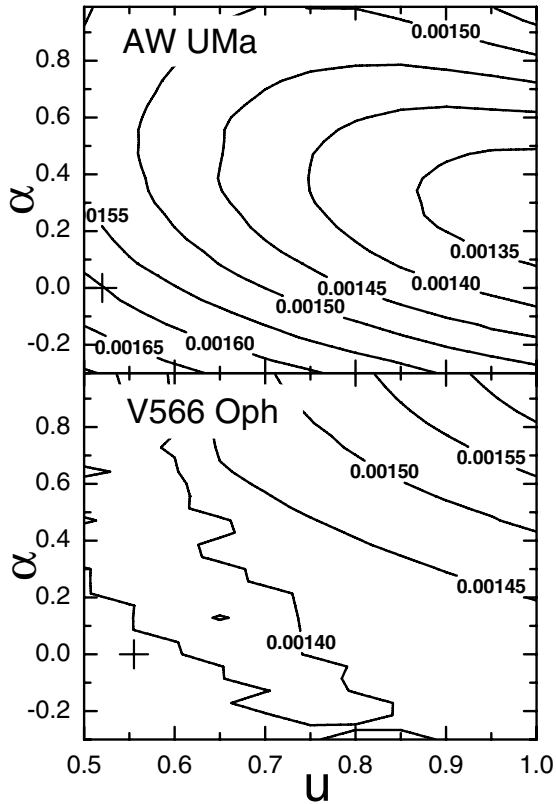
Figure 4. Results of a grid search for the limb darkening and differential rotation (u and α) coefficients best representing the observed BFs of AW UMa (top). The optimal fits occur for the highest permissible limb-darkening coefficient of $u = 1.0$ and $\alpha \approx 0.3$ (the pole rotating slower than equator). A similar plot for V566 Oph (bottom) shows a shallow minimum close to the nominal value of the limb darkening and of the solid body rotation (cross).

global minimum of weighted sum of squares of residuals for all BFs of AW UMa outside eclipses was performed within the domain $0.50 < u < 1.00$ and $-0.3 < \alpha < 1.0$. The orbital inclination of $i = 78.\!\!^\circ 3$ was adopted for AW UMa after Pribulla et al. (1999). The resulting dependence of χ^2 is shown in Fig. 4. It appears that the best fit can be obtained for an unphysical, large value of $u \rightarrow 1$ and for $\alpha \approx +0.3$; if a more physically acceptable value of u within $0.5 < u < 0.6$ was adopted, then the fits would require an even higher degree of the differential rotation with $\alpha \approx +0.55 \pm 0.05$. A similar grid search for V566 Oph in Fig. 4 shows a different behaviour. The dependence of χ^2 on both search parameters is rather weak and global minimum is not far from the expected limb darkening ($u = 0.56$) and solid-body rotation.

4.4 Direct modelling of the observed BFs using the contact model profiles

The approaches described above involved separate measurements of radial velocities for each component, to be later combined in a common spectroscopic orbit. One can go a step further. By fitting synthetic BFs to the observed ones – under an assumption of the Lucy contact model – the spectroscopic element determination is more direct; there is only one step of BF fitting which incorporates orbital parameters. In addition, this approach takes into account the proximity effects (such as deformation of components, gravity darkening and mutual irradiation) so that all available BFs can be

used, without a limitation to those with phases outside the eclipses. Such an approach was used successfully before for AW UMa and AH Vir by Rucinski (1992a) and Lu & Rucinski (1993).

The modelling of the BFs for AW UMa was performed assuming convective envelope for both components ($A_1 = A_2 = 0.50$, $g_1 = g_2 = 0.32$). The temperature of the primary was held fixed at $T_1 = 6980$ K, corresponding to spectral type F0V according to the calibration of Popper (1980). The temperature of the secondary, T_2, was coupled to T_1 through the gravity darkening law. The limb-darkening coefficients were interpolated in the tables of Van Hamme (1993) according to the mean surface temperature and gravity. The local surface fluxes were computed for the observed spectral range (5074–5306 Å). The optimized parameters were: the mass ratio q, fill-out factor F, sum of semi-amplitudes of radial velocities ($K_1 + K_2$), systemic velocity V_0 and temperature of the secondary T_2 (if decoupled from T_1 via gravity darkening law). We also adjusted the baseline level and normalization (scaling) of the BFs and the instant of the spectroscopic conjunction, T_0 (i.e. we did not use the pre-determined phases); the orbital period was, however, kept fixed at 0.438 7258 d. The synthetic BFs were smoothed by convolution with a Gaussian with $\sigma = 10.0$ km s^{-1} to exactly correspond to observational BFs (see Section 3). The phase smearing due to the length of exposures was taken into account by integrating the BFs over phase intervals corresponding to exposures with the integration step of 0.002 in phase. The extracted BFs of V566 Oph were modelled with similar assumptions, only T_1 was set to 6540 K to correspond to the F4V spectral type.

We found that a representation of the observed BFs of AW UMa by synthetic ones with the limb darkening taken from the tables of Van Hamme (1993), with T_2 coupled to T_1 through the local gravity darkening, results in a surprisingly poor match. First, we experienced problems similar to that for the rotational profile fitting in that the primary component showed a much more peaked signature than predicted. This may be taken as a proof that the difficulties described in Sections 4.2 and 4.3 were not caused by our neglect of the proximity effects, but were due to genuine deviations from the model. Secondly, with the direct fitting of the whole BFs, the difficulties were aggravated by the additional constraint of having the component temperatures, T_2 and T_1, closely linked through variations of the local gravity. The problem can be partially (if unphysically) resolved by making T_2 a free parameter and/or by assuming unrealistically high values of the limb-darkening coefficient and/or of the differential rotation. Each of these 'fixes' creates its own difficulties.

To fit the observed BFs by the model ones, we used several combinations of assumptions, but discuss here only three.

(i) A normal, i.e. expected atmospheric limb darkening, no differential rotation and the temperatures T_2 and T_1 coupled through the gravity-darkening.

(ii) A large value of the limb-darkening coefficient and T_2 decoupled from T_1.

(iii) A normal limb darkening, differential rotation and T_2 decoupled from T_1.

The last assumption requires an explanation. The differential rotation was modelled in a simple way by assuming the component shapes and the brightness distribution as predicted by the Roche model, and by modifying the rotational velocity according to the assumed, latitude-dependent, differential rotation law. Although this approach is not strictly consistent (the Roche model requires solid-body rotation) it is somewhat modelled on the Sun which remains spherical in the presence of the $\simeq 30$ per cent differential rotation.
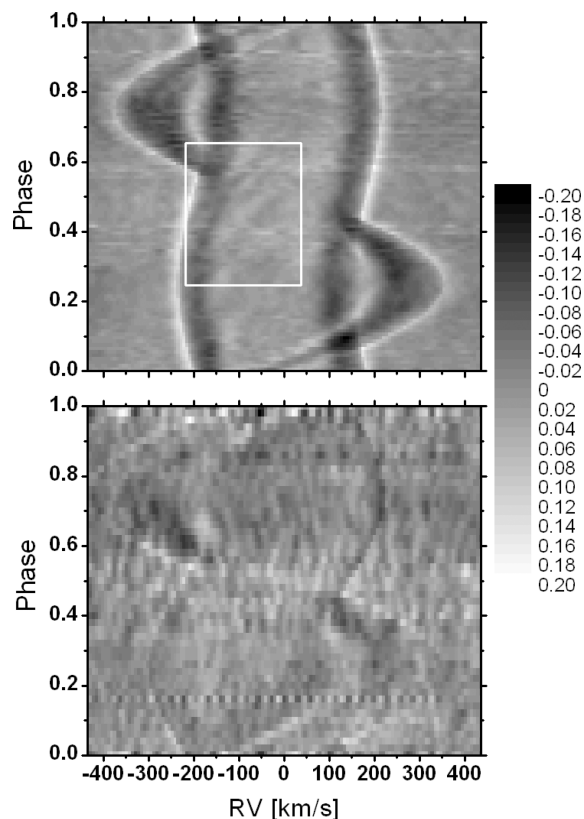
Figure 5. The map of residuals from the best fit to the observed BFs of AW UMa (top) and V566 Oph (bottom) using the direct BF fitting. For a comparison of both stars, the residuals are shown as deviations normalized to the respective maxima of the BFs so that the grey-scale applies to both panels. The 'kinks' in the AW UMa profiles, described in the text and marked in Fig. 2, are located at the place where the negative (dark) deviations suddenly change into positive (bright) ones. Although the secondary signature is always fainter than predicted, its transit in front of the primary (phase 0.0) does not appear as a dark trough, so that the secondary appears to have a similar temperature to that of the primary and a negligible limb darkening (however, we do see an asymmetry in the secondary transit, as commented in item 3 of Section 7). Note the diagonally drifting dark features in the AW UMa residuals (in the white box) which we interpret as photospheric spots. The most conspicuous spot emerges at the very left-hand edge of the profile so it must be located close to the equator of the primary component. The spots had to be stable over the one year of the full span in our observations to produce such a consistent picture. The residuals for V566 Oph do not show any systematic substantial deviations except a perturbation around phase 0.65.

We used α fixed at several values with the best fit for AW UMa obtained for $\alpha = 0.30$. The rebinned and smoothed residuals for the case (i) for both, AW UMa and V566 Oph, are shown in Fig. 5; the large systematic deviations for AW UMa should be noted, particularly in comparison with the almost ideal agreement with the contact model for V566 Oph. The final parameters of AW UMa for all considered cases are given in Table 4.

An inspection of the residuals of fits for AW UMa obtained under the above assumptions shows that the best representation is obtained for the case (ii) with $u_1 = 1.00$ and with T_2 decoupled from T_1 and thus individually optimized. Although this assumption is not physical, it does reproduce the observed shape of primary component signature the best. The secondary component always negligibly contributes to the overall value of weighted sum of residuals hence

its limb darkening could be always kept at the theoretically predicted value. It is interesting to note that for V566 Oph, the BFs can be modelled without any artificial assumptions (see Section 7 for discussion). The resulting spectroscopic elements of V566 Oph are close to those found from the same spectra in Pribulla et al. (2006) by using the rotational profile fits. While systemic velocity is practically the same, the sum of the semi-amplitudes, $K_1 + K_2$ is only about 1.6 per cent larger in the present, direct Roche model modelling.

5 SPECTROSCOPIC ELEMENTS AND THE ABSOLUTE PARAMETERS OF AW UMA

In order to determine the full range of uncertainties related to various methods of processing the radial velocity information, the spectroscopic elements for AW UMa were obtained first by simple sine-curve fits to individual radial velocities (Sections 4.1, 4.2, 4.3), then by direct fits to the whole BF profiles (Section 4.4). The results of the former are given in Table 3. The results of the direct BF fits are tabulated in Table 4, together with those for V566 Oph given for comparison.

The sine-curve fits were determined for the following cases: (1) the Gaussian fits, as described in Section 4.1, (2) the rotational profile fits with the expected limb darkening, $u = 0.52$ as described in Section 4.2, (3) the same, but with an artificially enhanced limb darkening, $u = 1.00$ and (4) rotational profile fits with $u = 0.52$, with a strong differential rotation characterized by $\alpha = 0.55$ (found by a grid search; see Fig. 4), as described in Section 4.3. The elements for the four cases are given as columns in Table 3. The phase diagram of radial velocities for case (3), best representing the observed BFs, is shown in Fig. 6.

A comparison of the Gaussian and rotational profile fits for BFs extracted around the orbital quadratures shows that the rotational profiles better represent the data. Moreover, Gaussian fits tend to overestimate the sum of semi-amplitudes, $K_1 + K_2$, and the total mass (see Table 3); this is caused by a 'cross-talk' in the sense that the wide wings of either of the components contribute to the profile of the other component. Especially, the secondary component position is driven away from the mass centre. Hence, we regard the spectroscopic elements derived by the Gaussian fits as biased. The rotational profile fits give markedly more consistent results with the final spectroscopic mass ratio, $q \approx 0.10$.

The contact model BF fits did not provide individual velocities of the components so that the orbital elements of the binary system were evaluated directly. We again considered various combinations of the limb-darkening coefficients (the expected ones as well as the enhanced one, $u = 1.0$, for the primary), as tabulated in Table 4. Again, the best representation of the observations was obtained with the strong limb darkening of the primary component. Even if the large limb darkening is not a correct assumption, it does give the best fits to the observed BFs. In the other two cases, χ^2 is dominated by differences in the predicted and observed shape of the primary; the least-squares fits ignore the shape of the secondary component and its semi-amplitude is incorrectly determined.

We summarize the results in Tables 3 and 4 by noting that while sum of semi-amplitudes $K_1 + K_2 \sim 325$ km s^{-1}, which leads to the total mass of the system of $M_1 + M_2 \simeq 1.5$–1.7 M$_\odot$ is consistent with values found by Rucinski (1992a), the spectroscopic mass ratio, $q \sim 0.1$, appears to be always larger than in the previous photometric investigations.

The absolute parameters of AW UMa, by necessity pertaining mostly to the primary component, suggest a moderate-mass star of

Table 3. Spectroscopic elements of AW UMa for three cases of the limb darkening and differential rotation (see text). Standard errors of parameters are given in parentheses.

Parameter Case	Gaussian (1)	Rotational (2)	Rotational (3)	Rotational (4)
u	–	0.52	1.00	0.52
α	–	0.0	0.0	0.60
V_0 (km s^{-1})	−9.17(0.77)	−8.64(0.53)	−8.83(0.61)	−8.76(0.54)
K_1 (km s^{-1})	28.45(0.92)	29.16(0.76)	29.81(0.77)	30.24(0.68)
K_2 (km s^{-1})	312.77(2.62)	299.77(1.03)	295.06(1.71)	295.5(1.68)
$K_1 + K_2$ (km s^{-1})	341.22(2.78)	328.93(1.28)	324.87(1.87)	325.74(1.81)
M_1(M$_\odot$)	1.655(40)	1.474(16)	1.415(24)	1.425(24)
M_2(M$_\odot$)	0.151(6)	0.143(5)	0.143(5)	0.146(4)
M_{12}(M$_\odot$)	1.806(40)	1.617(17)	1.558(25)	1.571(24)
$q = M_2/M_1$	0.091(3)	0.097(3)	0.101(3)	0.102(2)
$\sum w(O − C)^2$	1774.07	1454.3	1622.3	1483.3

Table 4. Parameters obtained by direct, Roche model BF fitting to the observed BFs of AW UMa and V566 Oph.

Parameter Case	AW UMa (1)	AW UMa (2)	AW UMa (3)	V566 Oph (4)
u_1	0.525	1.00	0.52	0.551
u_2	0.530	0.53	0.56	0.556
T_1 (K)	6980	6980	6980	6540
T_2 (K)	6901[a]	6201(9)	6475(28)	6478[a]
α	0.00	0.00	0.30	0.00
T_0 (HJD)	2 452 500.0315(1)	2 452 500.0315(1)	2 452 500.0313(1)	2 452 500.2537(1)
V_0 (km s^{-1})	−9.31(12)	−9.43(12)	−9.51(11)	−37.19(18)
Ω	1.9333(11)	1.9332(12)	1.9618(12)	2.2997(24)
Fill-out	0.256	0.353	0.304	0.435
$K_1 + K_2$ [km s^{-1}]	316.95(28)	333.66(32)	321.65(31)	346.58(49)
M_1(M$_\odot$)	1.405(4)	1.636(5)	1.499(26)	1.466(6)
M_2(M$_\odot$)	0.136(1)	0.162(1)	0.161(3)	0.378(2)
$q = M_2/M_1$	0.0969(5)	0.0990(4)	0.1079(4)	0.2575(11)
L_1(L$_\odot$)	5.88	6.53	5.92	3.65
L_1(L$_\odot$)	0.73	0.57	0.64	1.10
M_V (mag)	2.71	2.63	2.72	3.09
$\sum w(O − C)^2$	0.038 063	0.025 208	0.031 069	0.010 844

[a]T_2 recomputed from T_1 via the gravity darkening law. Standard errors of parameters are given in parentheses. Errors of masses are determined from the errors of $K_1 + K_2$ and q; the uncertainty in the inclination has been neglected.
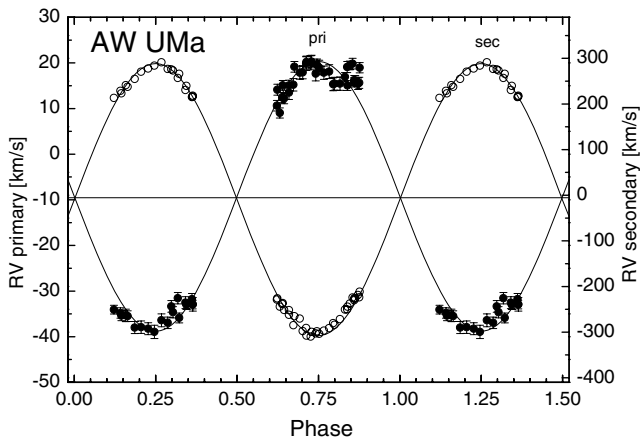
Figure 6. The radial velocity curves for the primary (full circles and the left-hand vertical axis) and the secondary component (open circles and the right-hand vertical axis) for AW UMa. The errors of radial velocities are shown for the primary component only; the formal errors for the secondary component are comparable with the size of symbols.

an advanced evolutionary state. The primary component mass, for the case of the high limb darkening, $M_1 = 1.636 \pm 0.005$ M$_\odot$ (the formal mean standard error), is compatible with the terminal-age main-sequence position. The combined absolute magnitude of AW UMa, $M_V = 2.63$ is compatible with the *Hipparcos* parallax and the distance estimated from the proper-motion companion (Table 1). We return to the matter of the absolute parameters of AW UMa in the last Section 9.

6 THE DIFFERENCE OF THE SPECTROSCOPIC AND PHOTOMETRIC MASS RATIO

In all light-curve solutions for contact binaries, determination of the photometric mass ratio is based on an assumption that both components are described by a common envelope corresponding to the same equipotential value within the Roche model. Geometrical relations for such a structure are entirely predictable and well known. Mochnacki & Doughty (1972a) pointed out that only two parameters, the mass ratio – entering via the ratio of radii – and the orbital

inclination uniquely determine the times of the inner eclipse contacts for totally eclipsing contact systems. This beautiful idea has worked numerous times for many contact binaries and has tremendously improved quality of light-curve solutions. As the currently ongoing spectroscopic program at the DDO (Pribulla et al. 2007) can attest, contact binaries which do not show total eclipses frequently have light-curve solutions giving entirely erroneous and useless values of q_{ph} when compared with the spectroscopic, direct determinations of q_{sp}. Thus, there is no reason to question such total-eclipse solutions as long as the main assumption of the Lucy model of the common equipotential in the *strict Roche model* is fulfilled. However, the common equipotential is still an assumption; if the secondary underfills its Roche lobe, then the photometrically determined mass ratio would be an underestimate of the actual value as the times of the inner eclipse contacts will be pushed to smaller phases.

Turning to the spectroscopic determinations of q_{sp}. Their main uncertainty is in the radial velocity semi-amplitude of the primary component, K_1, in $q_{sp} = K_1/K_2$, particularly when $q \to 0$. This results from $\delta_q^2 = (1/K_2)^2 \delta_{K_1}^2 + (q/K_2)^2 \delta_{K_2}^2$ where, for small q, the second term becomes irrelevant even when radial velocities of the secondary component are less accurate of the two ($\delta_{K_2} > \delta_{K_1}$). The masses and luminosities of the components, as given in Table 4, are consistent with this prediction.

7 OBSERVED DEVIATIONS FROM THE ROCHE MODEL

We clearly see several deviations from the strict Roche model predictions in our analysis of the BFs for AW UMa. They are documented in the BF residual maps, Fig. 5. The deviations are discussed mostly on the basis of our new spectroscopic material, but – to be sure of the consistency in our assumptions – we made also parallel analyses of the extant light curves of AW UMa utilizing the material and approaches as in Pribulla et al. (1999).

In what follows, we will use the term 'the primary (secondary) component' to describe the appearance of the respective stars in the BFs; this would be in place of the correct, but long expressions such as 'the primary (secondary) component signature as seen in the broadening functions'.

(1) *The primary component is too narrow and looks 'triangular'.* The central parts of the primary component are systematically too narrow than predicted by the contact model. The peaked shape of the primary BF is the reason why it could not be fitted by the normal limb-darkening law and required $u_1 \sim 1.0$ (Sections 4.3 and 4.4). A strongly differential rotation following the solar paradigm does not help much in alleviating this problem (solution #3 in Table 4) because the shape remains incorrect; particularly the 'kink' at 1/3 height (see the next item) is then even more prominent in the fit residuals.

An explanation by a very strong limb darkening does not have any good basis. The limb-darkening effect is a strictly local atmospheric phenomenon; it is very hard to force it to be larger because this would require an increase in the local gradient of the source function. If anything, the source function can be easily made flatter (e.g. due to local kinetic dissipation of horizontal motions or to magnetic energy deposition) so the limb darkening could be smaller than for normal, spherical stars rather than larger.

An explanation by the differential rotation would force us to reject the Roche model which is based on the solid-body rotation law. Application of a consistent, differentially rotating equivalent of the Roche model is beyond the scope of this study, mainly because

of the formidable theoretical obstacles how to treat the star shape and brightness distribution for such a case. In this paper, we use a hybrid model by retaining the Roche model for the shape and for the brightness prediction while artificially imposing a non-solid-body rotation law for velocities, but we stress that such a model is not internally consistent. We note that an introduction of a differential rotation characterized by the parameter $\alpha \neq 0$ in equation (1) was not fully satisfactory and the quality of the fits was inferior compared to assumption of a large limb darkening. Moreover, an explanation by a strong differential rotation or some steady surface circulation patterns (Motl, Frank & Tohline 2006) would require very rapid flows and strong velocity shear which – in turn – would cause shock waves in the photosphere, as argued by Anderson et al. (1983).

The 'triangular' shape of the primary is not seen by us for the first time. Anderson et al. (1983) and later Rucinski (1992a) appeared to see the same type of deviations. Synthesized spectra of AW UMa, including changes of local profile over the surface, by Anderson et al. (1983) showed that the variations of the surface temperature over the surface of the contact binary certainly cannot cause the peculiarity in the profile shape.

(2) *The primary component shows a wide 'base' or a large rotational-velocity 'pedestal'.* There exists an additional broadening at the base of the primary, reaching about 1/3 of its height above the baseline. It is enhanced by the pointed (triangular) shape of primary main peak. It does not have an obvious explanation, but it may be due to an equatorially distributed, hot matter, encompassing the whole system and possibly including the secondary within its extent. Due to the orbital inclination of AW UMa of only about $78°$, an equatorial belt should be visible through most of the orbital revolution, although at this point we cannot say much about its geometry. If the luminous matter is really there, its additional light in the system could explain the smaller than predicted (for $q = 0.10$) amplitude of the observed light curves of AW UMa (see item #5 below). However, the amount of light would have to be large ($L_3 = 0.14$) to drive the photometric mass ratio from $q \simeq 0.10$ to the popular value of the photometric mass ratio of ≈ 0.075.

(3) *The secondary component changes its shape with phase.* The secondary appears to be too small during the transit phases as if it was not a full, Roche filling star, but only a much smaller core. Its two sides (limb-darkened edges) are of unequal depths during the transit with the negative-velocity definitely darker. In addition, the secondary looks differently in the two orbital quadratures. It shows a faintly marked extension towards the primary at phases close to 0.25 while it appears to have a double structure (as if this star was itself a double or contained a rotating ring) at phases around 0.75. This is best visible in a comparison of the two orbital quadratures (Fig. 1). In addition, the shape of the secondary appears to vary in time-scales of perhaps weeks while the primary component remains remarkably stable in time. This variability is particularly well visible among spectra taken around phase 0.64 (Fig. 7).[2]

The orbital changes of the secondary component and particularly its small dimensions when projected against the primary may be interpreted in two ways: (i) either the secondary underfills its Roche lobe or (ii) what we see as a secondary is really an accretion region around a compact core. The small dimensions of the secondary would be consistent with the discrepancy between q_{sp} and q_{ph}, when the latter is determined through the phase of the inner eclipse contact.

---

[2] It should be noted that V566 Oph also shows a disturbance at phases close to 0.65; see the deviations from the model in Fig. 5.
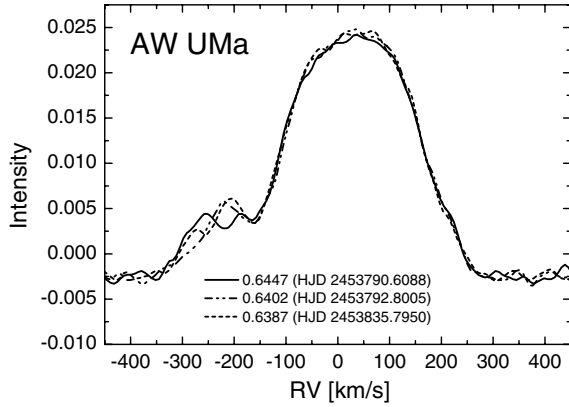
Figure 7. The temporal changes of the BF around the phase 0.64 of AW UMa. The epochs are separated by 2 and 43 d. Note that the phase region shown here corresponds to erratic behaviour of residuals in Fig. 5.

Figure 8. The synthetic spectrum of the Mg I feature in one of the orbital quadratures (phase 0.25), obtained by separately convolving BF contributions from each of the components of AW UMa represented by rotational profiles. The individual contributions are shown by dotted and dashed lines; resulting spectrum by a solid line. Note that placing the pseudo-continuum level at, say, 0.98 (which is what one would probably normally do) would have a much more profound effect on the definition of the secondary signature in the BF than on that of the primary component.

(4) *The secondary component is too faint and/or has a too low temperature.* The secondary component is too faint in the BFs as if the secondary was cooler than predicted. The required temperature to fit the secondary at quadratures would require a large temperature difference of components. For the assumed $T_1 = 7000$ K, it demands $T_2 = 6200$–6400 K. This is incompatible with observed light curves which show practically the same depth of minima. For instance Pribulla et al. (1999) assuming $T_1 = 7175$ K derived a similar $T_2 \sim 7000$ K.

The assumption of low T_2 helps to fit the secondary profiles around quadratures, but predicts a relatively deep cut into the profile of the primary component during its transit in front of the primary. This is not observed and the trough or depression during the transit (see Fig. 1) is very shallow, as if the temperature difference was in fact absent.

We suspect that this problem is not intrinsic to the star but may be due to difficulties with normalization of the AW UMa spectra prior to determination of BFs. Similarly as for other very close binaries, the spectra are notoriously difficult to handle in terms of an appropriate choice of the continuum level. This is because spectral lines in strongly rotationally broadened late-type spectra are heavily blended forcing one to define the local continuum relative to a basically arbitrary level between the lines. The importance of this effect can be illustrated by a simple experiment. We convolved the template spectrum with the expected contribution of each of the components of AW UMa at one of the orbital quadratures (phase 0.25). The result is shown in Fig. 8 where we see directly that the real continuum is entirely unknown. One must use a pseudo-continuum level with an uncertainty of at least 1–2 per cent.

Extensive tests of the BF technique have shown that shapes of the BFs are entirely unaffected by the uncertainty in the continuum level placement, but that the BF zero level may be shifted, usually to negative values (because the continuum is usually placed too low). The property of such simple shifts, without any influence on the shape, are due to the linear characteristics of the BFs and are a great advantage over the cross-correlation functions (where zero levels are usually not accessible at all). But the uncertainty of the zero level does influence integrated intensities of the two stellar peaks. It has practically negligible influence on the strength of the primary component in the BF, but – for a very small mass ratio – has a profound effect on the definition of the secondary peak as small differences in the zero level strongly influence its integrated strength.
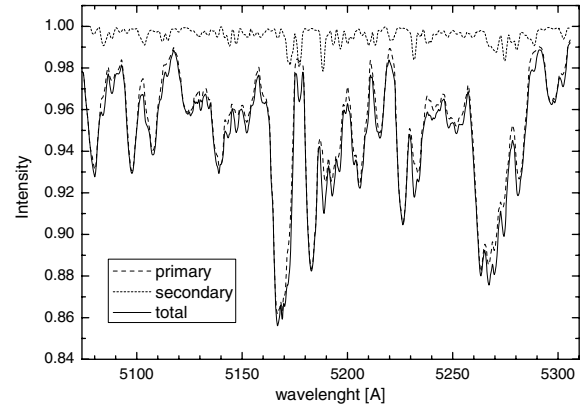
The effect is exactly in the direction of making the secondary too faint hence underluminous relative to the model.

(5) *There is an inconsistency in the amount of light in the system.* It is impossible to fit the observed light curves of AW UMa with the parameters derived from the radial velocity (BF) orbital solutions. The major obstacle is the predicted difference of the eclipse depths, $\delta m \approx 0.1$ mag, caused by different temperatures of components, which is not observed. The larger mass ratio, $q \simeq 0.10$ rather than 0.075, forces both minima to be deeper than observed. All previous photometric solutions were fully consistent with the smaller mass ratio and there was no contradiction between the elements. As already mentioned, this can be alleviated by the presence of an unaccounted third light in the system of about $L_3 \sim 0.14$. Except for indications of a luminous equatorial belt (item #2 above), we see no other possible light contribution. A decrease of the orbital inclination to solve the problem is out of the question because the light curve clearly shows total eclipses. We should stress, however, that our main conclusion concerning the mass ratio of $q \simeq 0.10$ is based solely on the radial velocity data and in no way is it related to the light amount budget evaluated from the eclipse depths.

(6) *The primary component is spotted.* The outer (away from the secondary) parts of the primary component reveal presence of unexplained dark features which run diagonally in the phase – radial velocity 2D diagram in Fig. 1 and can be interpreted as dark spots on a solid-body rotating primary. They are better visible in the picture of the residuals in Fig. 5. Their presence across the whole width of the primary component indicates that they must span the whole range of velocities, i.e. must be located close to the equator of the primary. They also contradict our suspicions of a differential rotation of the primary because they were apparently stabile over the whole period of one year. Obviously, we have no idea what is the origin of the features that we see; if these are magnetic spots, this would suggest a convective envelope which would be unexpected for the relatively early spectral type of AW UMa. We may note however that simple stellar structure arguments suggest that the primary should have a relatively deep convective envelope (Rucinski 1992b).

It should be stressed that the BF deviations from the Roche model – as seen in radial velocity maps – are definitely present and very well

defined for AW UMa, but are absent in V566 Oph (see e.g. Fig. 2). It seems that V566 Oph behaves fully according to the model and that it is AW UMa which appears to be in some way peculiar. This is all strange and unexpected, mostly because of the excellent agreement of the AW UMa light curve with the model. The two binaries have very similar spectral types and orbital periods, and differ really only in their mass ratios, $q = 0.10$ for AW UMa versus $q = 0.26$ for V566 Oph. Is this what causes the great difference between the systems and the strong deviations for AW UMa?

8 THE NEW MODEL FOR AW UMA

As described in the previous section, the secondary component of AW UMa, as seen in radial velocities, is far from what we would expect on the basis of the contact Lucy model. Because the secondary is faint and dominated by the much bigger and brighter primary companion, it is very hard to study, but its signature is definitely very different from that expected within the contact model. But the well observed primary is also showing major deviations from the contact model. We are absolutely sure now that (1) the span of the primary rotational velocities is much less than expected for the contact model and that (2) there is some additional source of continuum light at large rotational velocities relative to the primary centre (we call it 'the belt'). The problem (1) forced us to consider – as solutions – the unusually large limb darkening and the differential rotation field. But both are hard to accept, the former is not tenable on the grounds of what we know about stellar atmospheres while the latter cannot be reconciled with the presence of the photospheric spots strongly suggesting that the primary does rotate as a solid body.

We present here a radical and perhaps controversial suggestion. The primary (and probably the secondary) do not fill their common equipotential surface and they do not form a contact binary in the sense of Lucy's model. Our main argument is that the whole upper half of the primary BF can be ideally fit by the simple, solid-body rotational profile (Fig. 9). This fact, coupled with the perfectly rotationally synchronized dark spots on the primary, suggests that the primary is indeed a solid-body rotator with dimensions smaller than predicted by the contact model. The rotational broadening appears to be characterized by $V \sin i = 179.1 \pm 2.4$ km s^{-1} in the orbital quadratures and $V \sin i = 176.8 \pm 2.7$ km s^{-1} in the secondary minimum when the primary is seen 'from its end'. With the solid-body rotation, the 'side' dimension of the primary is R_1(side) $\simeq 1.58$ R$_\odot$. Thus, the primary's surface is close to, but some 15 per cent inside its *inner Roche lobe*. Changes of $V \sin i$ with the orbital phase (Fig. 10) for the primary component and for the belt indicate that while the primary is underfilling the inner Roche lobe, the belt may have dimensions comparable with the expected size of the contact model; this estimate includes the very risky assumption that the belt is also a solid-body rotator.

The assumption of the detached nature of the primary component cleanly solves the problem of the narrow, 'triangular' shape of the primary's BF, but at the cost of having to speculate about the 'belt'. We think that the belt may be an important source of light in the system; it is localized in the equatorial plane, it has the surface brightness properties (the temperature) not much different form those of the stellar surfaces, it must be optically and possibly also geometrically thick. *We stress that that the belt must produce an absorption spectrum, otherwise it would not be seen in the BF formalism.* There are absolutely no indications of any emission lines or of optical polarization (Piirola 1975, 1977); the presence of the latter could possibly suggest electron scattering of the stellar spectrum. Not much can be said about the secondary component in the new model, but in Section 7 we listed enough indications to think that it is quite abnormal.

In our picture (Fig. 11), both components are seen surrounded by the belt, but their mass centre velocities are not modified. Fits to
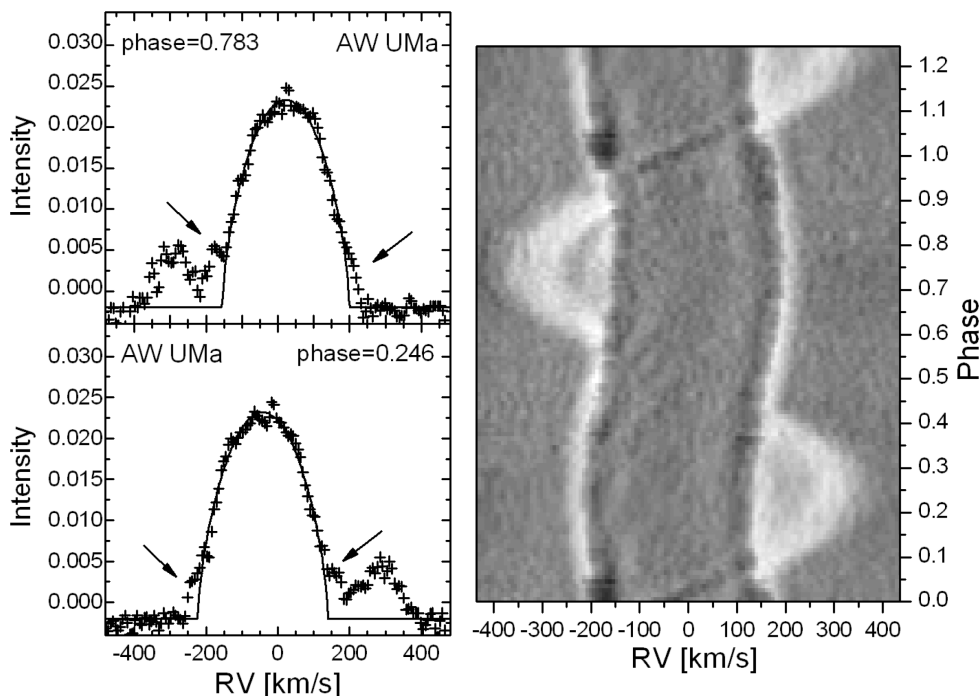

Figure 9. Fits to the upper halves of the primary signature are really excellent. Compare this figure with Fig. 2. Note that the additional broadening at the base, which we explain by the equatorial 'belt', is now even more prominent. The right-hand panel shows the deviations from rotational profile fits calculated for the primary component only (disregard the secondary component here). The belt around the primary is shown by the light-grey edge to the primary profile.
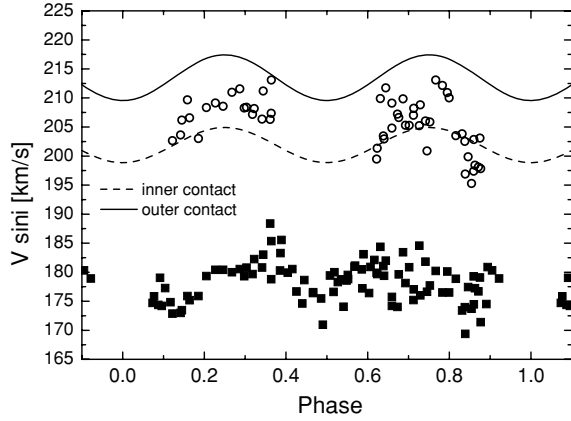
Figure 10. The phase dependence of projected rotational velocity $V \sin i$ for the primary component. The velocities were determined by rotational profile fits to the whole primary profiles, including the broadening due to the 'belt' (open circles) and to the upper halves of the profiles (squares). The theoretical rotational velocities of the primary component's inner and outer critical surfaces were computed assuming $K_1 + K_2 = 333.36 \, \text{km s}^{-1}$ for solution (2) in Table 4 with the fractional radii $r_{\text{side}} = 0.596$ and $r_{\text{back}} = 0.614$ with the orbital inclination angle of $78°\!.3$. The sine curves are simplified approximations of $V \sin i$ and are strictly valid for quadratures and conjunctions only. The whole profile fits were done only for phases outside ± 0.12 of the eclipses, while the upper-half fits excluded phases of the transit of the secondary component.
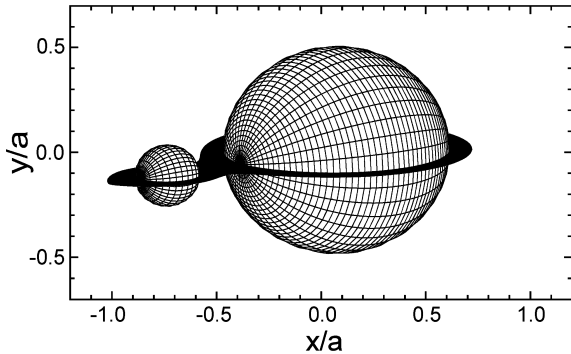

Figure 11. Typical look of AW UMa. The belt in this picture has the outer equatorial dimensions corresponding to the common equipotential for outer critical surface and may be thick while both stars are within their inner Roche lobes.

the upper halves of the primary give a well-defined value for $K_1 = 30.98 \pm 0.59 \, \text{km s}^{-1}$; this semi-amplitude is better defined than using any of the previous measurement techniques. Assuming the range of the K_2 semi-amplitudes as in the columns (2)–(4) of Table 3, we arrive at the masses $M_1 = 1.52$–$1.59 \, \text{M}_\odot$ and $M_2 = 0.159$–$0.164 \, \text{M}_\odot$. These are values practically identical to the ones determined previously, so the final elements of AW UMa are not changed at all. In particular, the mass ratio is basically the same, $q = 0.103$–0.104.

The question is: Why does photometry of AW UMa appear to be in such an excellent agreement with the Lucy model? And why does the binary appear so stable if it is so complicated? Frankly, we do not know. We prefer not to suggest any similarities of AW UMa to known peculiar binaries because such analogies may constrain future options in the interpretation. In this paper, we intended to show only well established observational facts limiting speculations

to a minimum. We note, however, that a period of a strong brightness instability of AW UMa was observed in 1989–1990 by Derman, Demircan & Müyesseroglu (1990). Thus, although the star seems to be normally stable and well behaving, this could be the time that the quiescent picture suddenly broke down.

9 SUMMARY

Our analysis of the BFs for the prototype of extreme mass ratio contact binaries, AW UMa, indicates that the generally accepted Roche model experiences major problems in interpretation of this system. We see strong indications that the system is not a contact binary and that both stars are smaller than their inner Roche lobes. The interpretation is complicated by the presence of what appears to be a luminous stream of the matter (optically thick and thus giving the same stellar spectrum), encompassing the primary and possibly the whole system and forming an equatorial belt around it. The equatorial extent of the belt is similar to the size of the common envelope derived in previous contact binary solutions.

The secondary strongly changes its spectroscopic appearance with the orbital phase and does not appear to be a normal star but rather a small stellar core surrounded by a complex disturbance of the belt. The primary is also showing unexpected deviations from the contact model. The 'triangular' or 'pointed' shape of the BFs (too narrow spectral lines) requires invoking an unusually strong limb darkening and/or a strongly differential rotation of the primary (the equatorial regions moving faster than polar). While the first explanation is unphysical, the second is inferior in terms of the overall fit to the data; it is contradicted by the presence of photospheric spots on the primary which were stable over one year. Our results and suggestions are radical ones because AW UMa – which appeared to be one of the best examples of the contact model – would not be then a contact binary in the sense envisaged by Lucy and by many researchers who followed his ideas. But we are driven to this desperate move only after exhausting all other alternatives.

A belt in the equatorial plane, encompassing both components is not an entirely new idea. In 1950, in his book Struve (1950) presented a picture (p. 188, fig. 28) which is very close to what we have in mind for AW UMa. Obviously, the new model would question the validity of the Lucy model for at least some binaries now considered to be in good contact. This is the price we appear to pay for having access to good spectral data and to improved methods of spectral analysis. Indeed, with only photometric information, and with the Lucy model, the realm of contact binaries has been not only amazingly appealing, but also much simpler.

We stress that irrespectively of assumptions used to describe the details of the whole picture, the radial velocities of the photocentres give the spectroscopic mass ratio of AW UMa close to $q_{\text{sp}} \simeq 0.10$. This value is significantly higher than the seemingly incontestable photometric mass ratio of $q_{\text{ph}} \simeq 0.07$–$0.08$. By taking global averages of our results, the masses of the components are approximately $M_1 = 1.5 \pm 0.15 \, \text{M}_\odot$ and $M_2 = 0.15 \pm 0.015 \, \text{M}_\odot$, where the uncertainties are estimated from systematic effects related to choices made in the analysis and are far larger than any of the formal uncertainty estimates for individual methods. Since the spectral data (in spite of several serious problems which we tried to stress rather than hide) directly give us radial velocities of the mass centres, the spectroscopic mass ratio of $q_{\text{sp}} \simeq 0.10$ must be close to the true one. The mass-ratio discrepancy, together with direct deviations from the expected velocity field, may be pointing to us a major deficiency in our assumptions about contact binaries. At this point we cannot state whether these deficiencies are *present* or are merely *best detectable*

only at the very low mass ratio of AW UMa. In either case, the deviations from the Roche/Lucy model appear to be highly significant for interpretation of contact binary systems.

This paper is dedicated to the memory of Bohdan Paczyński, the formidable teacher and towering intellect, but also an understanding colleague and friend. As a student, he discovered AW UMa in 1963 and recognized it as a particularly important one for understanding of contact binary stars. This star accompanied him over 44 yr of his immensely productive astronomical life to his last contribution which he directly supervised (Paczyński et al. 2007).

REFERENCES

Anderson L., Standford D., Leininger D., 1983, ApJ, 270, 200
Derman E., Demircan O., Müyesseroglu Z., 1990, IBVS, 3540
European Space Agency, 1997, The *Hipparcos* and Tycho Catalogues (ESA SP-1200). ESA Publications Division, Noordwijk
Høg E. et al., 2000, A&A, 355, L27
Lu W., Rucinski S. M., 1993, AJ, 106, 361
Lu W., Rucinski S. M., 1999, AJ, 118, 515
Lucy L. B., 1968a, ApJ, 151, 1123
Lucy L. B., 1968b, ApJ, 153, 877
McLean B. J., 1981, MNRAS, 195, 931
Mochnacki S. W., Doughty N. A., 1972a, MNRAS, 156, 51
Mochnacki S. W., Doughty N. A., 1972b, MNRAS, 156, 243
Motl P. M., Frank J., Tohline J. E., 2006, BAAS, 38, 118
Paczyński B., 1964, AJ, 69, 124
Paczyński B., Sienkiewicz R., Szczygieł D. M., 2007, MNRAS, 378, 961
Piirola V., 1975, Inf. Bull. Var. Stars, 1060
Piirola V., 1977, A&A, 56, 105
Popper D. M., 1980, ARA&A, 18, 115
Pribulla T., Rucinski S. M., 2006, AJ, 131, 2986
Pribulla T., Chochol D., Rovithis-Livaniou H., Rovithis P., 1999, A&A, 345, 137
Pribulla T. et al., 2006, AJ, 132, 769
Pribulla T., Rucinski S. M., Conidis G., DeBond H., Thomson J. R., Gazeas K., Ogłoza W., 2007, AJ, 133, 1977
Pych W., 2004, PASP, 116, 148
Rensing M. J., Mochnacki S. W., Bolton C. T., 1985, AJ, 90, 767
Rucinski S. M., 1992a, AJ, 104, 1968
Rucinski S. M., 1992b, AJ, 103, 960
Rucinski S. M., 2002, AJ, 124, 1746
Rucinski S. M., Duerbeck H. W., 1997, PASP, 109, 1340
Rucinski S. M. et al., 2005, AJ, 130, 767 (DDO-X)
Struve O., 1950, Stellar Evolution: An Exploration from the Observatory. Princeton Univ. Press, Princeton, NJ
Tokovinin A. A., Smekhov M. G., 2002, A&A, 382, 118
Van Hamme W., 1993, AJ, 106, 2096

SUPPLEMENTARY MATERIAL

The following supplementary material is available for this article:

Table 2. Journal of spectroscopic observations of AW UMa and V566 Oph. [Correction added after online publication 26 March 2008: Table 2, not Table 1, is available as supplementary material. The table caption has been corrected accordingly.]

This material is available as part of the online article from: http://www.blackwell-synergy.com/doi/abs/10.1111/j.1365-2966.2008.13033.x (this link will take you to the article abstract).

Please note: Blackwell Publishing are not responsible for the content or functionality of any supplementary materials supplied by the authors. Any queries (other than missing material) should be directed to the corresponding author for the article.

This paper has been typeset from a TEX/LATEX file prepared by the author.